Mechanical properties of electrodeposited nanocrystalline and ultrafine-grained Zn-Sn coatings

Mahsa Esfahani, Khurram S. Munir, Cuie Wen, Jie Zhang, Yvonne Durandet, James Wang, Yat Choy Wong

PII: S0257-8972(17)31101-5
DOI: doi:10.1016/j.surfcoat.2017.10.059
Reference: SCT 22824

To appear in: *Surface & Coatings Technology*

Received date: 10 April 2017
Revised date: 5 October 2017
Accepted date: 22 October 2017

Please cite this article as: Mahsa Esfahani, Khurram S. Munir, Cuie Wen, Jie Zhang, Yvonne Durandet, James Wang, Yat Choy Wong , Mechanical properties of electrodeposited nanocrystalline and ultrafine-grained Zn-Sn coatings. The address for the corresponding author was captured as affiliation for all authors. Please check if appropriate. Sct(2017), doi:10.1016/j.surfcoat.2017.10.059

Mechanical properties of electrodeposited nanocrystalline and ultrafine-grained Zn-Sn coatings

Mahsa Esfahani[a,*], Khurram S. Munir[b], Cuie Wen[b], Jie Zhang[c], Yvonne Durandet[a], James Wang[a], Yat Choy Wong[a]

[a]Faculty of Science, Engineering and Technology, Swinburne University of Technology, Hawthorn, Victoria 3122, Australia

[b]School of Engineering, RMIT University, Melbourne, Victoria 3001, Australia

[c]School of Chemistry and Australian Research Council Centre of Excellence for Electromaterials Science, Monash University, Clayton, Victoria 3168, Australia

*Corresponding author.

E-mail address: mesfahani@swin.edu.au (M. Esfahani)

Phone: +61 468 933 859; Fax: +61 3 9214 5050

Abstract

This study investigates the effects of grain size on the mechanical properties of Zn-Sn alloy coatings. Nanocrystalline (average grain size = 78 ± 18 nm) and ultrafine-grained (average grain size = 423 ± 96 nm) Zn-Sn coatings were electrodeposited on steel substrates from gluconate electrolytes containing organic additives. The microstructure, surface roughness and mechanical properties of electrodeposited coatings were investigated using field emission scanning electron microscopy (FE-SEM), three dimensional (3D) surface profilometry, nano-hardness, nano-scratch and nano-wear tests. The average surface amplitude parameters such as mean surface roughness (S_a) and root mean square roughness (S_q) decreased by at least 80% while, hardness increased from 209 ± 66 MPa to 523 ± 140 MPa, due to grain refinement from ultrafine-grained to nanocrystalline structure. Nano-scratch results indicated that a deeper grove was formed on the surface of ultrafine-grained coatings than

nanocrystalline coatings during the sliding process. For both coatings coefficient of friction increased gradually over the entire sliding duration and reached to maximum of 0.24 ± 0.04 and 0.12 ± 0.02 in ultrafine-grained and nanocrystalline coatings respectively. Wear volume of the coatings decreased by 64.5% due to grain refinement from ultrafine-grained to nanocrystalline structure.

Keywords:

Electrodeposition, Nanocrystalline, Ultrafine-grained, Nano-hardness, Nano-scratch, Nano-wear

1. Introduction

The steel industry comes after oil and gas as the second largest industry in the world. World growing population has led to the increase of steel use per capita from 150 kg in 2001 to 208 kg in 2015, and it is predicted that the demands for use would increase by 1.5 times higher than present levels by 2050 [1]. However, the sustainability of steel products is at risk due to corrosion and wear. Coatings are one of the acceptable methods for protection of steel structures. Thus, fabrication of coatings with improved properties will always be beneficial to the steel industry.

It is well-known that the properties of materials vary as a function of grain size [2, 3]. Since Gliether's first introduction of nanocrystalline material in 1984 [4], numerous studies have been conducted to investigate the effects of grain refinement down to nano-scale on the properties of materials. In many cases, nanocrystalline materials show advanced mechanical [5-7] and chemical [8] properties in comparison to polycrystalline counterparts, which make them a point of interest for many studies and applications.

Zinc-tin alloy coatings provide sacrificial properties of zinc and barrier properties of tin against corrosion to steel substrate. Also, these coatings are used for protection of steel parts that undergo deformation due to their good frictional properties and excellent ductility [9]. Improvement of corrosion and mechanical properties of zinc [10-12] and some of zinc alloys such as zinc-nickel [13-15] due to grain refinement to nano-scale has been previously reported. However, to the best knowledge of the authors, the effects of grain refinement on the mechanical properties of zinc-tin coatings has not been previously reported. Therefore, the main aim of this study is to evaluate the effects of grain refinement from ultrafine-grained to nanocrystalline microstructure on the mechanical properties of Zn-Sn coatings.

Generally, various techniques are used for the synthesis of nanocrystalline materials from vapour, solid and liquid routes [16]. Electrodeposition is an economical technique from a liquid route which has been used to produce nanocrystalline metals and alloys [17]. In this technique increase in nucleation rate and decrease in grain growth (requirements of nanocrystallization) are controlled by applying a pulse current and use of organic additives [18-20].

In this study nanocrystalline (NC) and ultrafine-grained (UFG) Zn-Sn coatings were synthesized from environmentally friendly gluconate electrolyte using pulse electrodeposition in the presence of hexadecyltrimethylammonium bromide (CTAB) and polyethylene glycol (PEG) with average molecular mass of 2050 g/ mol and 400 g/ mol, respectively. The surface morphology, grain size and composition of the coatings has been evaluated prior to the evaluation of mechanical properties of the coatings.

2. Experimental

2.1. Sample preparation

Nanocrystalline (NC) and ultrafine-grained (UFG) Zn-Sn coatings were prepared by pulse electrodeposition in a 150 ml three-electrode cell under stationary conditions using a CHI electrochemical workstation. A platinum mesh (20 mm × 20 mm) and a Ag/AgCl (1M KCl) electrode were used as the counter electrode and the reference electrode, respectively. Mild steel discs with a surface area of 1.13 cm^2 were used as the working electrodes. The Ag/AgCl reference electrode was placed closed to the working electrode to minimize the influence of uncompensated resistance. Before deposition, the discs were polished to mirror finish, then sonicated in ethanol for 5 minutes followed by rinsing with distilled water. The polished discs were pickled in 10% HCl for 10 s, then rinsed with distilled water and dried using N_2 flux. The disc was then placed in the plating electrolyte immediately after cleaning to avoid contamination. Table 1 shows the chemical composition of the solutions and the plating conditions used to produce the Zn-Sn coatings. The average thickness of the coatings was 11.6 ±1.3µm.

Table 1. List of the plating solutions and plating conditions.

2.2 Characterization

A ZEISS Supra 40 VP field emission scanning electron microscope (FESEM) fitted with an energy dispersive X-ray spectrometer (EDS, Oxford Instrument, INCA Energy 250) were used for the characterisation of the deposits' surface morphology and elemental composition. Atomic force microscope (AFM) Multimode 8 (Bruker) at intermittent contact mode was used to image the surface of nanocrystalline coating. Average grain size of the deposit was measured from AFM and SEM cross section images. In both methods ImageJ software was

used to measure the grain sizes. Grains were identified as discrete areas which were separated from the adjacent neighbor by boundaries. In most cases grains did not have a symmetrical geometry therefore the biggest length of the grain geometry was measured as the representative of the grain size. At least three SEM images of each samples were used for grain measurements.

X-ray diffraction analysis was performed using a Bruker D8 Advance X-ray diffractometer with Cu Kα radiation (**λ**=0.15418 nm), working at 40 mA and 40 kV at a rate of 0.2˚ min^{-1} over the diffraction angle (2θ) range of 10-90º.

Surface profile measurements were performed using a Contour GT-K, Bruker Nano, 3D profilometer (USA) coupled with SurfVision software. The average surface amplitude parameters of the NC and the UFC were measured by scanning 2 fresh samples of each coatings at 10 different locations.

The nano-mechanical properties of the fabricated coatings, e.g., hardness, scratch and wear, were investigated using a Hysitron TI-950 TriboIndenter with a Berkovich diamond tip on the surface of as-deposited coatings.

To measure nano-hardness and modulus of elasticity, load was applied in a series of trapezoidal loading cycles with a total cycle of 20 on different positions (array of 5 × 4). The maximum load for each cycle was incrementally increased with each loading cycle with the first cycle having a maximum load of 50 μN and last cycle having a maximum load of 1000 μN. Each load was applied linearly up to maximum load in 10 s with a dwell time of 10 s followed by unloading in 10 s. For each coating, twenty indentations were performed in the form of 5 × 4 array at 3 different locations on 2 fresh samples. The indentations were separated by 20 μm to avoid the effect of any residual stresses. Thermal drift was set to be less than 0.05 nm/s. The nano-hardness and elastic modulus of the coatings were evaluated using Oliver and Pharr method [21].

The nano-scratch test was performed at the load controlled mode and at a constant load of 100 μN. The test was repeated for three times for each of the NC and UFG coatings. Fig. 1 shows the load function applied in this study.

Fig. 1 Normal applied force versus time.

The tribological properties of the fabricated coatings were assessed by conducting nano-wear tests by Hysitron Triboindenter instrument with methods described in previous studies [22-24]. The diamond indenter tip scanned a specific area of 5 × 5 (μm^2) under a constant force of 100 μN to perform wear on the surface of the coating. The scanning wear test was performed by scrapping the selected area by 10 sliding passes. A post wear-scan was then conducted on the same scanned area at a reduced force of 2 μN. The resultant worn volume was then calculated from the obtained image by the height difference from the unworn and worn surfaces using Hysitron Triboview software. The total wear volume in the coatings was calculated through the following relations.

|Height outside wear region [nm]| - |Height inside wear region [nm]| = Wear height [nm]

(Square of wear scan size [μm^2]) × (wear height [μm]) = Wear volume [μm^3]

3. Results

Surface morphology, microstructure and grain size of the NC and UFG coatings are characterized and evaluated to provide a comprehensive insight of the coatings before evaluating mechanical properties in later stages of this study.

3. 1. Surface morphology, microstructure and grain size

Fig. 2 shows the surface morphology, cross section and EDS spectra of the NC and the UFG Zn-Sn coatings. Nanocrystalline materials have grains smaller than 100 nm in which a great number of atoms belong to the grain boundaries or interfacial boundaries. Surface morphology of the NC coating (Fig. 2a) exhibits a uniform structure of nano grains packed together tightly with some protruding areas. The average grain size of the NC coatings as measured from the surface AFM imaging (Fig. 3a) and cross-sectional SEM images was 78 ± 18 nm. Surface morphology of the UFG coatings composed of closely packed grains. Average grain size of the UFG coatings as measured from the surface AFM imaging (Fig. 3b) and cross-sectional SEM images of the coatings was 423 ± 96 nm. The average zinc and tin contents of the alloys are presented in the inset of Fig. 2.c and f. Data shows that the two coatings have very close chemical compositions. EDS spectra of the coatings exhibit major peaks of tin, zinc and minor peaks of oxygen and iron. Iron peaks comes from the steel substrate.

Fig. 2 Characteristics of the NC (a, b and c) and the UFG (d, e and f) Zn-Sn coatings. (a and d) SEM images of the surface morphology, (b and e) SEM images of the cross-section and (c and f) corresponding EDS spectra.

Fig. 3 AFM image of the surface of the (a) NC and (b) UFG coatings.

Elemental maps of the surfaces of the NC and the UFG coatings (Fig. 4) are performed on the surface of as-deposited coatings to find the coloration between nano-hardness (section 3.3.1) and chemical composition of the coatings. It is observed that Zn and Sn have both dispersed across the surface in a nonhomogeneous pattern. There are some regions in Fig 4 (c and f)

that are rich in tin and slightly depleted from zinc. Rich tin areas possibly formed during the deposition process due to small gradient of the potential on the surface of electrode caused by the absorption and desorption of additives. It has to be noted that zinc and tin exhibit very small mutual solubility based on their phase diagram [25], therefore Zn-Sn is considered as a mechanical type of alloy in which zinc and tin do not form a solid-solution or an intermetallic compound and only form a mechanical mixture of hexagonal zinc and tetragonal β-Sn phases. X-ray diffraction patterns of NC and UFG coatings is presented in Fig. 5 and reveals a mixture of hexagonal zinc and tetragonal βSn phases.

Fig. 4 Surface SEM images of (a) the NC coating and (d) the UFG coating and corresponding elemental X-ray analyses of zinc in (b) NC and (e) UFG. (c) and (f) tin elemental X-ray analyses in the NC and the UFG coatings, respectively.

Fig. 5 XRD patterns of the NC and UFG coatings.

The average crystallite size of the deposits were calculated according to Scherer's equation [26].

$$D = 0.9\lambda/B\cos\theta \quad (1)$$

Where D is the average crystallite size, λ is the X-ray wavelength, *B* is the full width at half maximum (FWHM) of a diffraction peak and θ is the diffraction angle [26].

The average crystallite size of NC and UFG coatings are 24.52 ± 8.38 and 102.73 ± 23.16 respectively.

3. 2. Three-dimensional Optical Profilometry

Evaluation of the surface profile of a deposit is important due to its effects on the wear properties and friction coefficient of the deposit. Normally, rough surfaces have higher

coefficient of friction and wear quickly. Therefore, surface roughness measurement can help with the prediction of mechanical properties of the coatings.

3D profilometry images of the NC and the UFG Zn-Sn coatings are presented in Fig. 6a and b, respectively. The average surface amplitude parameters of the NC and the UFC are presented in Table 2.

Fig. 6 3D profilometry images of (a) NC and (b) UFG Zn-Sn deposits. Vertical bar shows the amplitude range per image (20 K X magnification, 0.32 × 0.24 mm imaged area).

Table 2. Surface amplitude parameters of the NC and the UFG Zn-Sn deposits.

3. 3. Mechanical properties of nanocrystalline and ultrafine-grained Zn-Sn coatings

3. 3. 1. Nano-hardness and elastic modulus

Nanoindentation was conducted to evaluate the hardness and elastic modulus of the NC and the UFG Zn-Sn coatings. Fig. 7 shows typical nanoindentation load-displacement curves of the coatings. Red circles in Fig. 7 represent the pop in events which are explained later in the manuscript (section 4).

Fig. 7 Typical load-displacement curves for nanoindentation of (a) NC and (b) UFG Zn-Sn coatings.

The average nano-hardness and elastic modulus of the coatings are presented in Table 3.

Table 3. Nano-hardness and elastic modulus of the NC and the UFG Zn-Sn coatings.

Three dimensional (3D) hardness maps which describe hardness of the coatings as a function of indentation positions on a sample are presented in Fig. 8.

The maps show that hardness has not been uniformly distributed across the surface. This is mainly linked to nonhomogeneous distribution of zinc and tin across the surface (see Fig. 4). Zinc has higher modulus of elasticity (104.5 GPa [27]) than tin (44.3 GPa [27]), therefore, it is expected that rich zinc areas show higher hardness than tin rich areas. Thus, red zones in Fig. 8 which reflect high hardness are attributed to zinc rich areas and purple and blue zones are attributed to tin rich areas.

Fig. 8 3D hardness maps of (a) NC and (b) UFG Zn-Sn coatings.

3. 3 .2 Nano-scratch

The main purpose of performing a nano-scratch test is to determine the coefficient of friction of the coatings. Fig. 9 a and b are nano-scratch plots of the coatings and show normal displacement and coefficient of friction as a function of time, respectively.

Fig. 9 (a) Normal displacement and (b) coefficient of friction as a function of time for the NC and the UFG Zn-Sn coatings.

For evaluation of the results, it has been considered that the relevant part of the friction test is from 10 s to 42 s, as before 10 s the load was ramping from 0 to 100 µN, and after 42 s the load was decreasing to zero. Curve of the normal displacement versus time (Fig. 9 a) showed that for the equal amount of load (100 µN) which was applied during the friction test on both NC and UFG coatings, a deeper groove was formed on the surface of the UFG. In general, the average depth of scratch of the UFG coating was 64% higher than that of NC coating. The

coefficient of friction of the NC coatings increased from 0.03 at 10 s to 0.12 at 42 s, while the coefficient of friction of the UFG coatings increased from 0.10 at 10 s to 0.24 in 42 s (Fig. 9 b). Although for both coatings, the coefficient of friction increased with time, the coefficient of friction of the UFG coating increased with higher rate than of the NC coating.

3. 3. 2 Wear properties

Surface hardness, microstructure and coefficient of friction are some of the parameters which have effects on the wear properties of materials. Wear is a damage that can be produced by relative motion of a surface and a contacting substrate. Abrasion wear occurs when a hard member moves on a softer surface by digging or grooving [28] .Fig. 10 shows SEM images of the worn area of the NC and the UFG Zn-Sn coatings. In both cases the wear is abrasive as the diamond indenter tip is much harder than the NC and the UFG coatings. The wear volume decreased by 64.5% due to grain refinement from the UFG to the NC coatings.

Fig. 10 SEM images of (a) NC and (b) UFG Zn-Sn coatings. (C) wear volume of the coatings after 10 sliding passes under 100 μN load applied on a 5 μm × 5 μm scan area.

4. Discussion

The arithmetic average height parameter (Sa) denotes the average absolute value of the height (roughness irregularities) within a sampling area. Sq, denotes the root mean square value of the surface departures, within the sampling area. Surface profilometry results showed that S_a and S_q of the NC coatings are at least 80% smaller than the UFG coatings, which shows that surface amplitude paraments are linked to grain size and surface morphology of the deposits. Surface morphology of the NC coating is consisted of fine grains packed together smoothly, however, surface morphology of the UFG is accumulation of larger grains. The skewness

(S_{sk}) indicates the degree of symmetry of the surface deviation about the mean reference plane. A negative skewness indicates that the surface has more pores than peaks, and positive sign shows vice versa. The value of the skewness of both NC and UFG deposits was negative (-0.15 ± 0.03 in NC and -0.44 ± 0.09 in UFG). Absolute values of the skewness of the NC is smaller than the UFG Zn-Sn deposits which indicates that less pores exist in the NC than the UFG structure. This is due to the different molar mass of PEG used to synthesis the NC and the UFG Zn-Sn deposits (PEG 2050 and PEG 400 were used for the synthesis of the NC and the UFG deposits, respectively) and their effects on hydrogen evolution. During the electrodeposition of Zn-Sn from aqueous solutions, hydrogen evolution occurs simultaneously with metal deposition and leads to pore production. Surfactants are mainly added to the electroplating solutions to form an absorbed layer on the surface of substrate to aid the detachment of the hydrogen bubbles from the surface. The absorption of PEG occurs through its oxygen atoms, and strength of the absorbed layer on the surface of electrode depends on number of oxygen atoms [29]. PEG 2050 has higher number of oxygen atoms than PEG 400, therefore, it can form a stronger absorbed layer. As a result, recombination of H atoms and release of H_2 occurs more effectively in the presence of PEG 2050 (NC coating) than PEG 400 (UFG coating) and led to the decrease of the absorption of H_{ads} to the surface of electrode. Consequently, less pores were produced during the deposition of the NC than the UFG coatings, and thus the absolute value of skewness of NC is smaller than UFG coatings.

Typically, in nanoindentation, with the increase of load the increase in displacement (penetration depth) are observed. However, in our study the increase in displacement with the increase of load was not observed for the NC or the UFG coatings occasionally (Fig. 7), which was mainly due to non-homogeneous distribution of zinc and tin across the coatings (Fig. 4). Elemental mapping of the coatings showed that there were areas rich in either tin or

zinc. This difference in the distribution of tin and zinc across the coating led to variation in indentation behavior and irregular distribution of hardness (Fig. 8) as described in 3.3.1 section.

On the other hand, it has been reported [30] that under constant load, the load-displacement curve for two different grains of tin with various orientation showed significantly larger displacement for the (100) plane than the (110) plane due to higher elastic modulus of (100) plane (58 GPa) than (110) plane (50 GPa). Therefore, the occasional anomalous decrease in displacement despite the increased load suggests that; during the indentation, from one point to another, either indenter has moved from a rich tin area to the position depleted from tin and rich in zinc, (which is inherently harder than tin) or if the subsequent area is still rich in tin, then most of tin grains are orientated along (110) planes that have higher modulus of elasticity and leads to the reduction of displacement.

Some of the load-displacement curves show traces of pop-in events (red circles in Fig. 7 show examples of these pop-in events). Pop-in events are considered as the initiation of plastic behavior on a loading process during indentation [31]. The pop-in phenomena are interpreted as the nucleation of dislocations and occur if the maximum shear strength produced under the indenter is of the same magnitude as the theoretical shear strength. Then this localized high shear strength leads to nucleation of dislocations and produces a displacement discontinuity in the load-displacement curve [32].

Hardness of material is a function of the grain size according to Hall-Petch equation [33] (Equation 2). Hardness increases with decreasing grain size down to 15 nm, after which the reverse of the Hall-Petch effects emerge.

$$H = H_i + K_{H-P}\, d^{\frac{-1}{2}} \qquad (2)$$

Where H is the hardness, H_i is the lattice friction stress, $K_{H\text{-}P}$ is the Hall-Petch constant and d is the grain size. Increase in hardness values with the decrease of grain size has been reported

in literature [34-38] and it has mainly been explained based on the relation of grain size and grain boundaries. Generally, decrease in grain size leads to the increase in grain boundaries. It has been reported [39] that volume fraction of grain boundaries could be around 50% for grain smaller than 5 nm and decreases to 10% and 1% with the increase in grain size to 50 nm and 1µm, respectively. The grain boundaries act as a barrier to the movements of dislocations and thereby inhibit plastic deformation and leads to the increase of hardness. In this study the decrease in grain size from 423 ± 96 nm to 78 ± 18 nm led to an increase of hardness in accordance to Hall-Petch equation and a nearly constant elastic modulus. Slight decrease of elastic modulus is only reported at grain size less than 20 nm, above this threshold of the grain size no significant change in elastic modulus has been reported[40]. Results of nano-scratch test (Fig. 9) was in accordance with the nano-hardness result. The lower hardness of the UFG coatings (209 ± 66 MPa) compared to the NC coatings (523 ± 140 MPa) results in a lower resistance to deformation and allows a deeper groove to be produced for the same values of force on the surface of the UFG coatings during the sliding process. The increase in friction coefficient of the coatings with time is the effect of piling up of wear debris formed at the time of sliding in front of the scratching tip. The lower gradient (slope) of the friction curve of the NC than the UFG showed that less coating was detached from the sample during the scratching process and indicated that the NC coatings have a higher cohesion bonding than the UFG coatings.

Wear analysis (Fig. 10) showed a decrease in wear volume from 13.4 ± 3.7 μm^3 in the UFG to 4.7 ± 1.6 μm^3 in the NC which is in agreement with Archard's law. Based on Archard's Law of Wear (Equation 3) [41], at a constant applied load, an increase in hardness leads to a decrease in wear volume.

$$W = K\frac{L}{H} \qquad (3)$$

Where W is volume worn per unit sliding distance; L is the applied load; H is the hardness of the softer of the materials in contact (Zn-Sn coating in this study), and K is a dimensionless constant. As it was observed in section 3.3.1, the NC coatings showed a higher hardness (523 ± 140 MPa) than the UFG (209 ± 66 MPa) coatings. Therefore, at the constant applied load of this study (100 μN) the decrease in wear volume of the NC than the UFG coatings is expected based on Archard's Law. These results are also consistent with the lower coefficient of friction of the NC coatings than the UFG coatings [42].

SEM images of the NC and the UFG coatings after wear analysis (Fig. 10) shows that materials are piled up during the sliding process for the NC coatings. However, UFG coatings did not show any effects of pile up. During the wear test, sliding contact induces significant compression and shear at asperities, leading to large plastic deformations even at low applied loads. As the diamond indenter moves on the surface, the removal of softer materials occurs and leaves grooves or scratches behind. The wear debris travels along the sliding track and piles up at the end of each track. The initial stage of wear is different from the wear after a few passes due to the variation in surface roughness. At the beginning the ploughed coating moves to the valleys of the surface and after a few passes the surface becomes smoother [24] . It was observed that the absolute value of the skewness of the NC was smaller than that of UFG deposits (-0.15 ± 0.03 in the NC and -0.44 ± 0.09 in the UFG), which indicated the NC coatings have smaller number of pores and valleys than the UFG coatings. Therefore, the ploughed UFG coatings had more opportunities than the ploughed NC coatings to fill up the pores and valleys. The NC ploughed coatings are built-up at the end of wear track, while, grains are flattened and gaps between grains are filled with sheared material and debris (plastically deformed) at the UFG coatings.

4. Conclusion

Physical and mechanical properties of nanocrystalline and ultrafine-grained Zn-Sn coatings were evaluated in this study. Influence of grain size on surface roughness, hardness and tribological behavior of the NC and the UFG coatings were studied. The NC coatings exhibited superior mechanical properties such as higher hardness, lower coefficient of friction and smaller wear volume than the UFG coatings. Both NC and UFG have either rich tin or rich zinc areas on their structure which leads to nonhomogeneous distribution of hardness on the surface. Modulus of elasticity were not affected by grain refinement and remained almost constant after grain refinement.

Acknowledgment

This study was partly supported by AutoCRC which is one of the Australian Government's Cooperative Research Centers.

The authors acknowledge the facilities, and the scientific and technical assistance of RMIT University's Microscopy and Micro-analysis facility, a lined laboratory of the Australian Microscopy & Microanalysis Research Facility.

References

[1] (April 2017). www.worldsteel.org.

[2] R. W. Armstrong, "The influence of polycrystal grain size on several mechanical properties of materials," *Metallurgical and Materials Transactions,* vol. 1, pp. 1169-1176, 1970.

[3] K. D. Ralston and N. Birbilis, "Effect of grain size on corrosion: A review," *Corrosion,* vol. 66, pp. 0750051-07500513, 2010.

[4] H. Gleiter and P. Marquardt, "Nanocrystalline Structures - An Approach to New Materials?," *Zeitschrift fuer Metallkunde/Materials Research and Advanced Techniques,* vol. 75, pp. 263-267, 1984.

[5] M. A. Meyers, A. Mishra, and D. J. Benson, "Mechanical properties of nanocrystalline materials," *Progress in Materials Science,* vol. 51, pp. 427-556, 2006.

[6] N. Wang, Z. Wang, K. T. Aust, and U. Erb, "Effect of grain size on mechanical properties of nanocrystalline materials," *Acta Metallurgica Et Materialia,* vol. 43, pp. 519-528, 1995.

[7] J. Liu, X. Zhou, X. Zheng, H. Cui, and J. Zhang, "Tribological behavior of cold-sprayed nanocrystalline and conventional copper coatings," *Applied Surface Science,* vol. 258, pp. 7490-7496, 7/15/ 2012.

[8] L. Liu, Y. Li, and F. Wang, "Electrochemical Corrosion Behavior of Nanocrystalline Materials—a Review," *Journal of Materials Science & Technology,* vol. 26, pp. 1-14, 1// 2010.

[9] E. Budman and R. R. Sizelove, "Zinc alloy plating," *Metal Finishing,* vol. 97, pp. 334-339, 1999.

[10] K. M. S. Youssef, C. C. Koch, and P. S. Fedkiw, "Improved corrosion behavior of nanocrystalline zinc produced by pulse-current electrodeposition," *Corrosion Science,* vol. 46, pp. 51-64, 2004.

[11] Q. Li, H. Lu, J. Cui, M. An, and D. Li, "Electrodeposition of nanocrystalline zinc on steel for enhanced resistance to corrosive wear," *Surface and Coatings Technology,* vol. 304, pp. 567-573, 2016.

[12] Q. Li, Z. Feng, J. Zhang, P. Yang, F. Li, and M. An, "Pulse reverse electrodeposition and characterization of nanocrystalline zinc coatings," *RSC Advances,* vol. 4, pp. 52562-52570, 2014.

[13] S. H. Mosavat, M. H. Shariat, and M. E. Bahrololoom, "Study of corrosion performance of electrodeposited nanocrystalline Zn–Ni alloy coatings," *Corrosion Science,* vol. 59, pp. 81-87, 6// 2012.

[14] G. Y. Li, J. S. Lian, L. Y. Niu, and Z. H. Jiang, "Microstructure and performances of nanocrystalline zinc-nickel alloy coatings," *Cailiao Rechuli Xuebao/Transactions of Materials and Heat Treatment,* vol. 25, pp. 1275-1278, 2004.

[15] G. Y. Li, J. S. Lian, L. Y. Niu, and Z. H. Jiang, "Investigation of nanocrystalline zinc-nickel alloy coatings in an alkaline zincate bath," *Surface and Coatings Technology,* vol. 191, pp. 59-67, 2005.

[16] C. Suryanarayana, "Structure and properties of nanocrystalline materials," *Bulletin of Materials Science,* vol. 17, pp. 307-346, 1994.

[17] U. Erb, "Electrodeposited nanocrystals: Synthesis, properties and industrial applications," *Nanostructured Materials,* vol. 6, pp. 533-538, 1995.

[18] G. Devaraj, S. Guruviah, and S. K. Seshadri, "Pulse plating," *Materials Chemistry and Physics,* vol. 25, pp. 439-461, 1990/08/01 1990.

[19] M. S. Chandrasekar and M. Pushpavanam, "Pulse and pulse reverse plating—Conceptual, advantages and applications," *Electrochimica Acta,* vol. 53, pp. 3313-3322, 3/10/ 2008.

[20] W. Plieth, "Additives in the electrocrystallization process," *Electrochimica Acta,* vol. 37, pp. 2115-2121, 1992.

[21] W. C. Oliver, "An improved technique for determining hardness and elastic modulus using load and displacement sensing indentation experiments," *Journal of Materials Research,* vol. 7, pp. 1564-1583, 1992.
[22] Z. Jiang, C.-J. Lu, D. Bogy, and T. Miyamoto, "An investigation of the experimental conditions and characteristics of a nano-wear test," *Wear,* vol. 181, pp. 777-783, 1995.
[23] K. S. Munir, Y. Zheng, D. Zhang, J. Lin, Y. Li, and C. Wen, "Microstructure and mechanical properties of carbon nanotubes reinforced titanium matrix composites fabricated via spark plasma sintering," *Materials Science and Engineering: A,* vol. 688, pp. 505-523, 3/14/ 2017.
[24] J. Chen, S. J. Bull, S. Roy, A. Kapoor, H. Mukaibo, H. Nara*, et al.*, "Nanoindentation and nanowear study of Sn and Ni-Sn coatings," *Tribology International,* vol. 42, pp. 779-791, 2009.
[25] H. ASM, Ed., *ASM handbooks online* Materials Park, Ohio : ASM International 2003, p.^pp. Pages.
[26] B. D. Cullity, *Elements of X-ray Diffraction*, 2nd ed.: Addison-wesley 1978.
[27] W. Callister, *Materials science and engineering : an introduction*, 7th ed. New York, NY: John Wiley & Sons 1940.
[28] E. Rabinowicz, *Friction and wear of materials*, 2nd ed.. ed. New York: New York : Wiley, 1995.
[29] L. Mirkova, G. Maurin, I. Krastev, and C. Tsvetkova, "Hydrogen evolution and permeation into steel during zinc electroplating; effect of organic additives," *Journal of Applied Electrochemistry,* vol. 31, pp. 647-654, 2001.
[30] A. Campbellová, P. Klapetek, V. Buršíková, M. Valtr, and J. Buršík, "Small-load nanoindentation experiments on metals," *Surface and Interface Analysis,* vol. 42, pp. 766-769, 2010.
[31] T. Ohmura, L. Zhang, K. Sekido, and K. Tsuzaki, "Effects of lattice defects on indentation-induced plasticity initiation behavior in metals," *Journal of Materials Research,* vol. 27, pp. 1742-1749, 2012.
[32] C. A. Schuh, "Nanoindentation studies of materials," *Materials Today,* vol. 9, pp. 32-40, 2006.
[33] A. H. Chokshi, A. Rosen, J. Karch, and H. Gleiter, "On the validity of the hall-petch relationship in nanocrystalline materials," *Scripta Metallurgica,* vol. 23, pp. 1679-1683, 1989/10/01 1989.
[34] G. W. Nieman, J. R. Weertman, and R. W. Siegel, "Mechanical behavior of nanocrystalline Cu and Pd," *Journal of Materials Research,* vol. 6, pp. 1012-1027, 1991.
[35] J. Chen, L. Lu, and K. Lu, "Hardness and strain rate sensitivity of nanocrystalline Cu," *Scripta Materialia,* vol. 54, pp. 1913-1918, 2006.
[36] M. Furukawa, Z. Horita, M. Nemoto, R. Z. Valiev, and T. G. Langdon, "Microhardness measurements and the hall-petch relationship in an Al-Mg alloy with submicrometer grain size," *Acta Materialia,* vol. 44, pp. 4619-4629, 1996.
[37] G. D. Hughes, S. D. Smith, C. S. Pande, H. R. Johnson, and R. W. Armstrong, "Hall-petch strengthening for the microhardness of twelve nanometer grain diameter electrodeposited nickel," *Scripta Metallurgica,* vol. 20, pp. 93-97, 1986.
[38] C. Suryanarayana and C. C. Koch, "Nanocrystalline materials – Current research and future directions," *Hyperfine Interactions,* vol. 130, pp. 5-44, 2000.
[39] G. Palumbo, S. Thorpe, and K. Aust, "On the contribution of triple junctions to the structure and properties of naoctystalline materials," *Scripta metallurgica,* vol. 24, pp. 1347-1350, 1990.
[40] J. D. Giallonardo, U. Erb, K. T. Aust, and G. Palumbo, "The influence of grain size and texture on the Young's modulus of nanocrystalline nickel and nickel-iron alloys," *Philosophical Magazine,* vol. 91, pp. 4594-4605, 2011.
[41] J. F. Archard, "Contact and Rubbing of Flat Surfaces," *Journal of Applied Physics,* vol. 24, pp. 981-988, 1953.

[42] P. C. King, R. W. Reynoldson, A. Brownrigg, and J. M. Long, "Pin on disc wear investigation of nitrocarburised H13 tool steel," *Surface Engineering,* vol. 21, pp. 99-106, 2005/04/01 2005.

Table 1. List of the plating solutions and plating conditions.

Solutions	Constituents	Plating Conditions
Nanocrystalline coating (NC)	0.45 M Na-Gluconate ($C_6H_{11}Na\ O_7$) + 0.56 M Na_2SO_4+ 0.18 M HCl + 0.04 M $SnCl_2$ + 0.4 M $ZnSO_4$,7 H_2O + 1 mM CTAB + 1 g/l PEG ($\bar{M}_n$= 2050)	T = 21 ± 1 °C $t_{on\text{-}time}$ = 5 ms, $t_{off\text{-}time}$ = 7 ms Current density = 0.046 A/cm^2 Plating time = 1200 seconds pH = 4.3-4.7
Ultrafine-grained coating (UFG)	0.45 M Na-Gluconate ($C_6H_{11}Na\ O_7$) + 0.56 M Na_2SO_4+0.18 M HCl+ 0.04 M $SnCl_2$ + 0.4 M $ZnSO_4$,7 H_2O + 1 mM CTAB + 4 g/l PEG ($\bar{M}_n$= 400)	T = 21 ± 1 °C $t_{on\text{-}time}$ = 5 ms, $t_{off\text{-}time}$ = 7 ms Current density = 0.046 A/cm^2 Plating time = 1200 seconds pH = 4.3-4.7

Table 2. Surface amplitude parameters of the NC and the UFG Zn-Sn deposits.

Deposit	S_a (nm)	S_q (nm)	S_{sk} (au)
Nanocrystalline	105 ± 19.4	137 ± 25.5	-0.15 ± 0.03
Ultrafine-grained	561 ± 50.6	694 ± 62.0	-0.44 ± 0.09

Table 3. Nano-hardness and elastic modulus of the NC and the UFG Zn-Sn coatings.

Deposit	Nano-hardness (MPa)	Elastic Modulus (GPa)
Nanocrystalline	523 ± 140	59.1 ± 15
Ultrafine-grained	209 ± 66	59.9 ± 11

List of Figures

Fig. 1

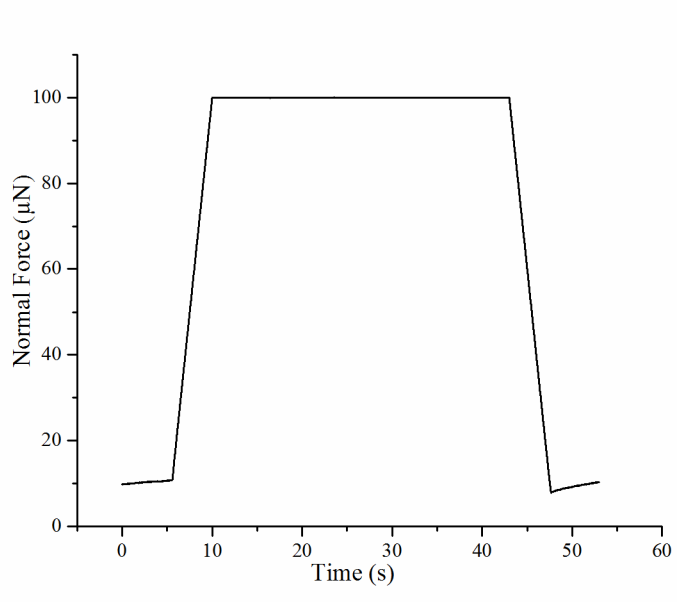

Fig. 2

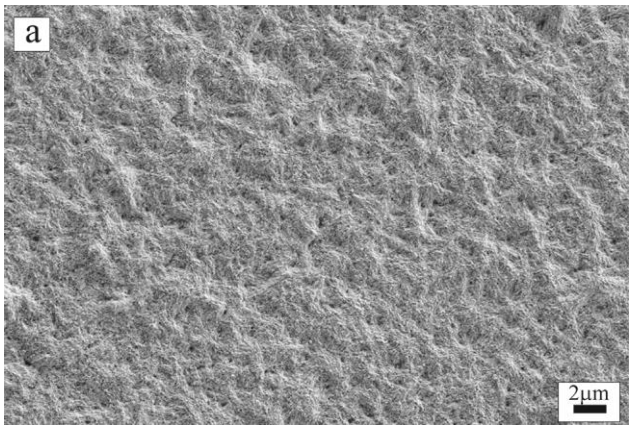

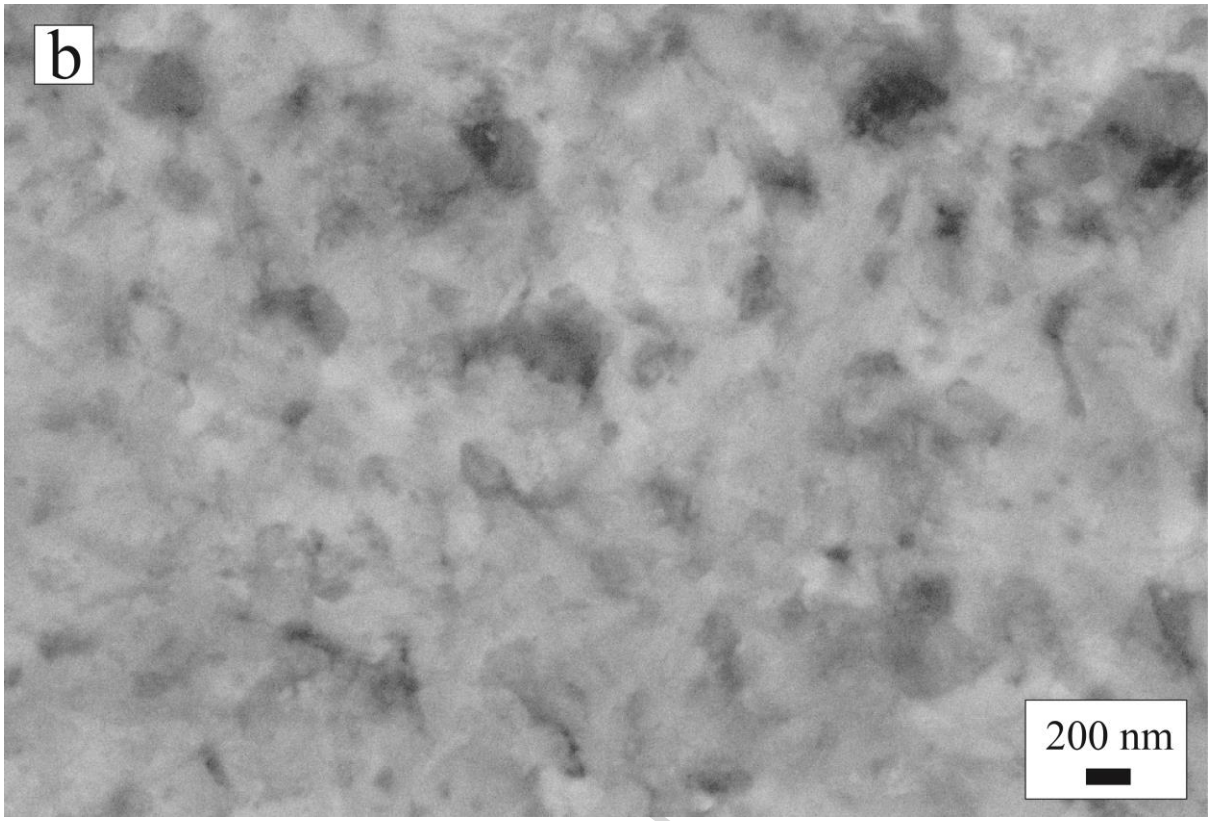

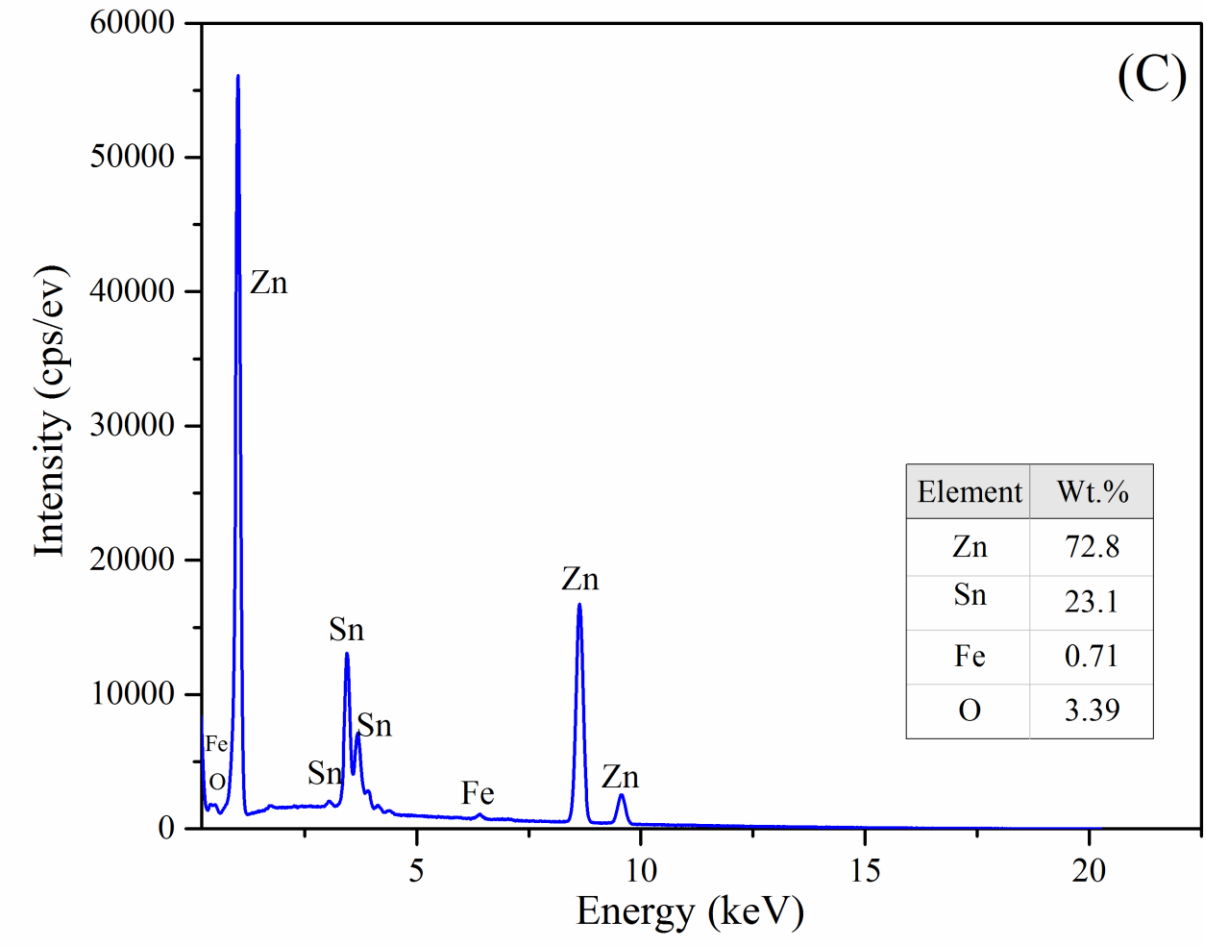

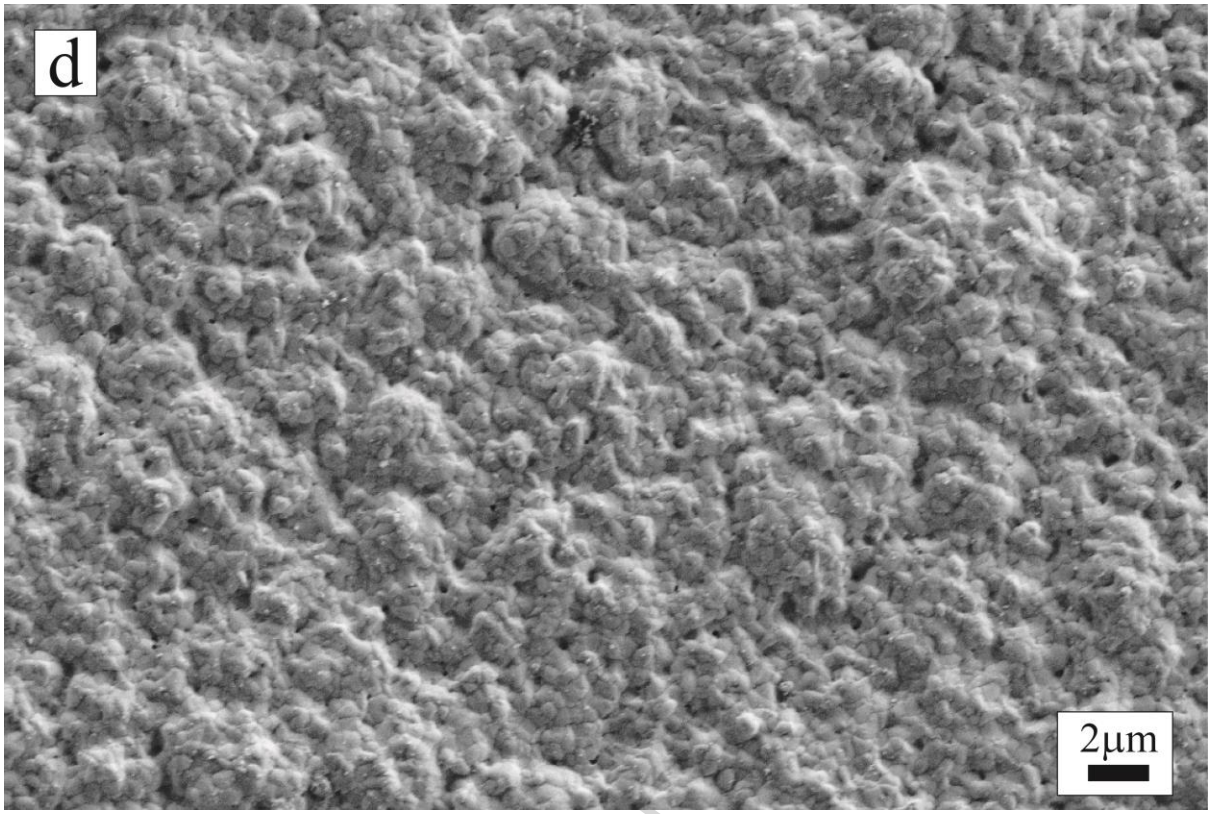

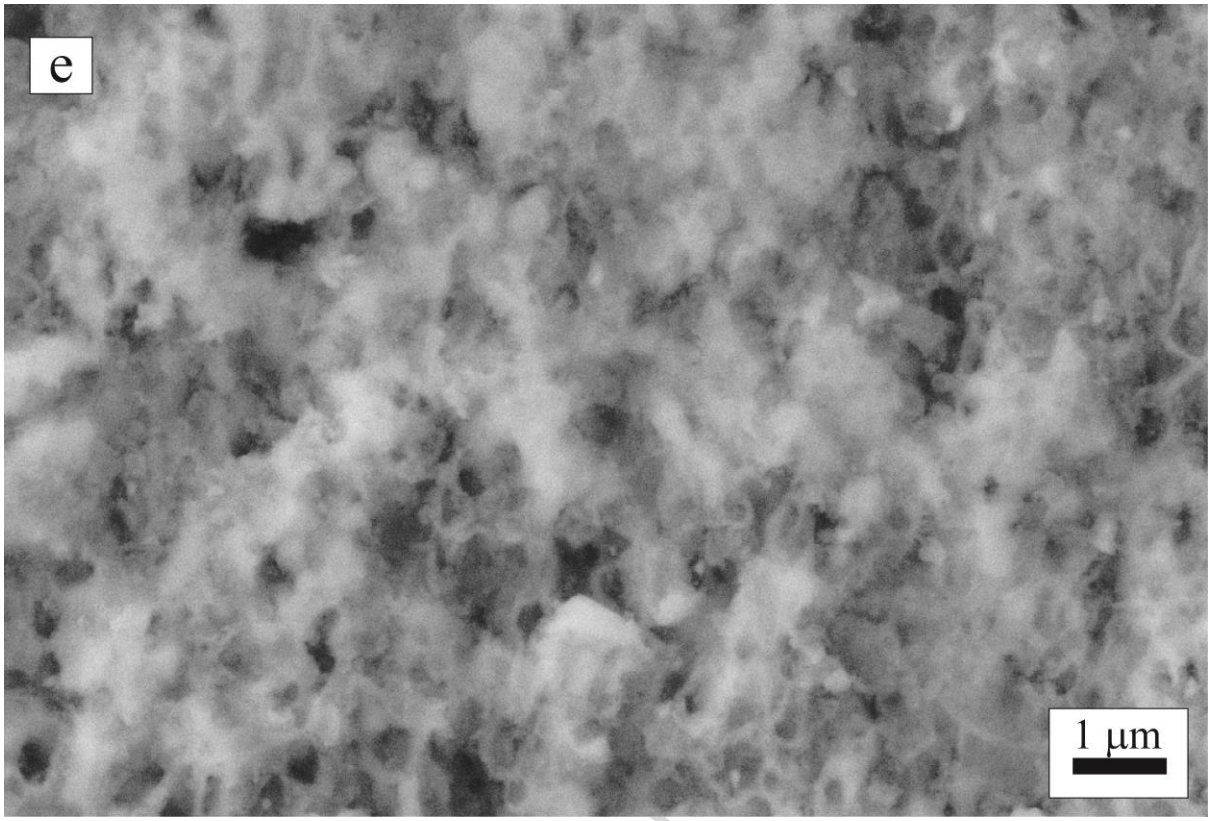

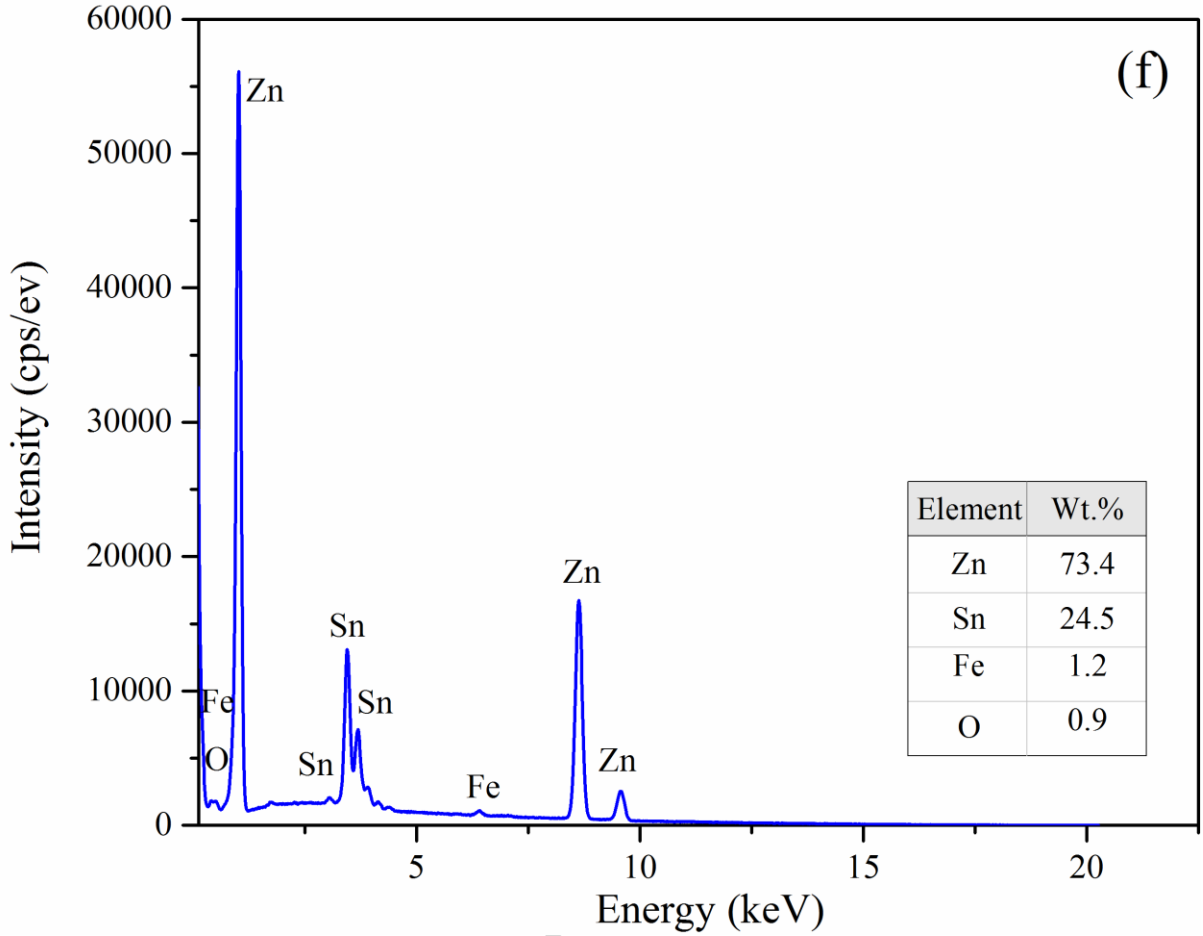

Fig. 3a

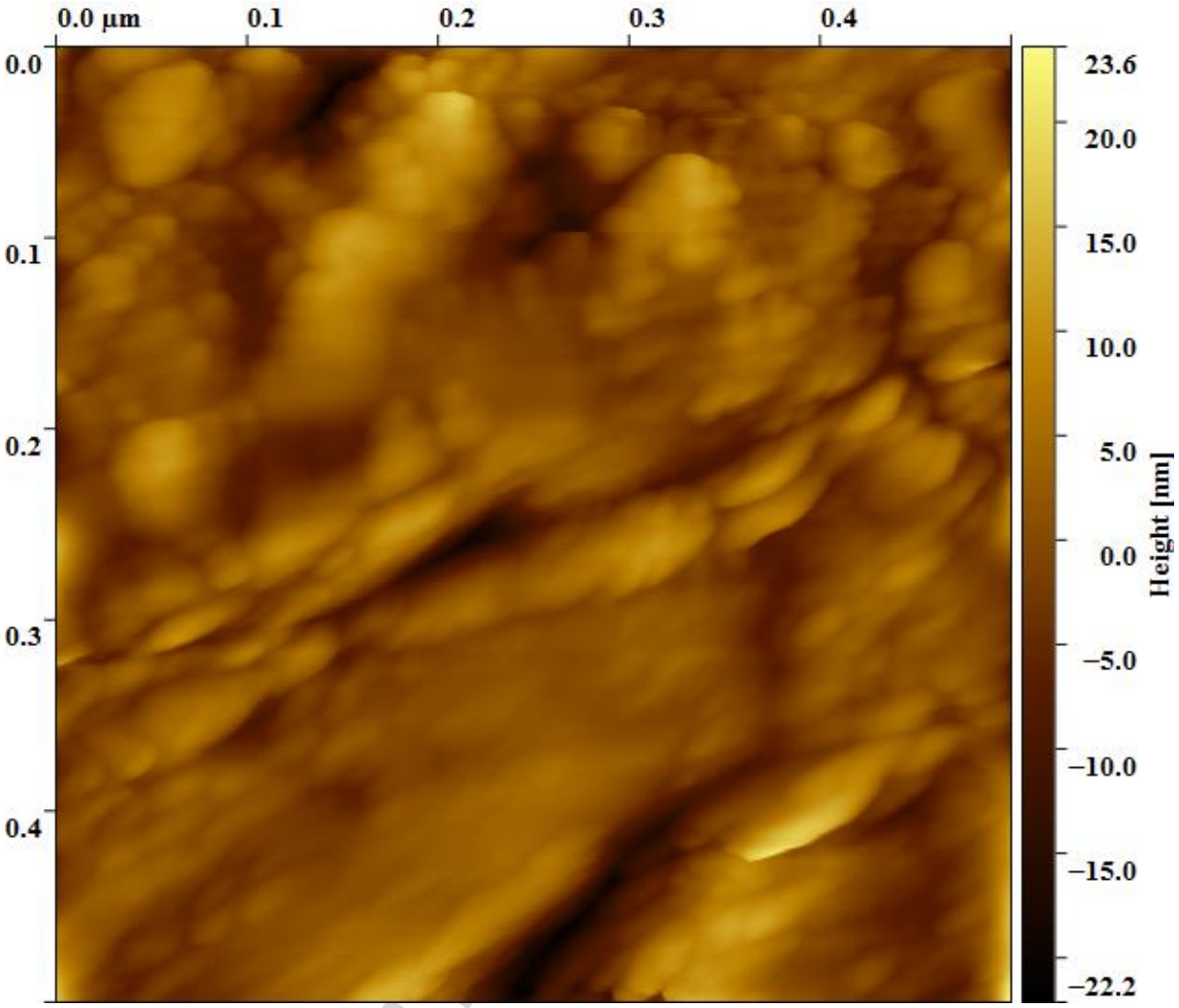

Fig. 3b

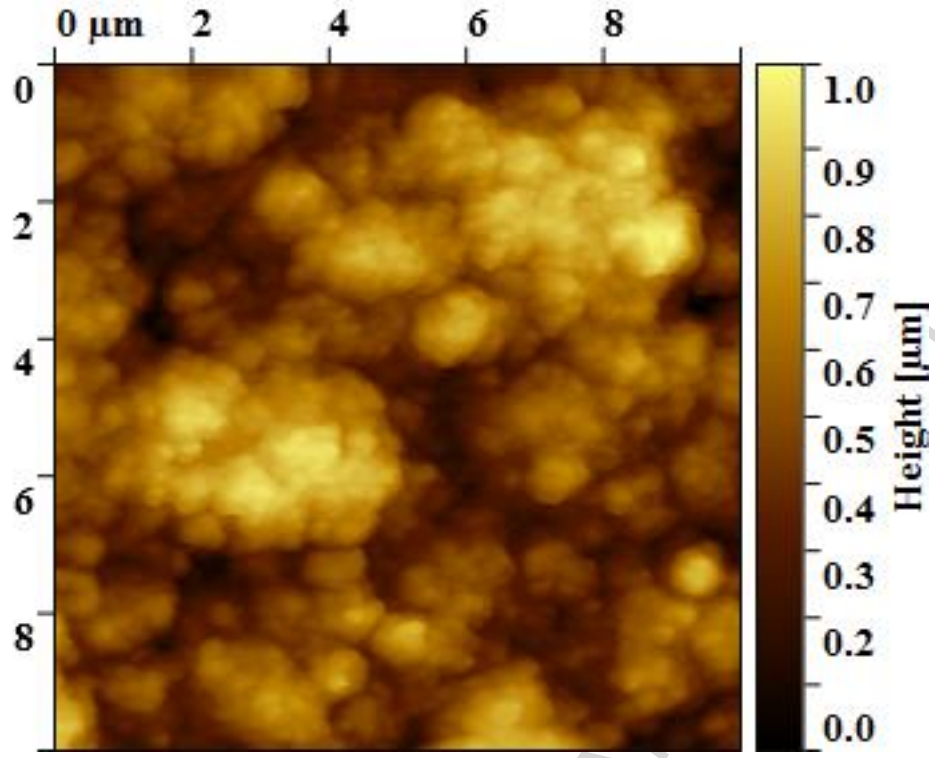

Fig. 4

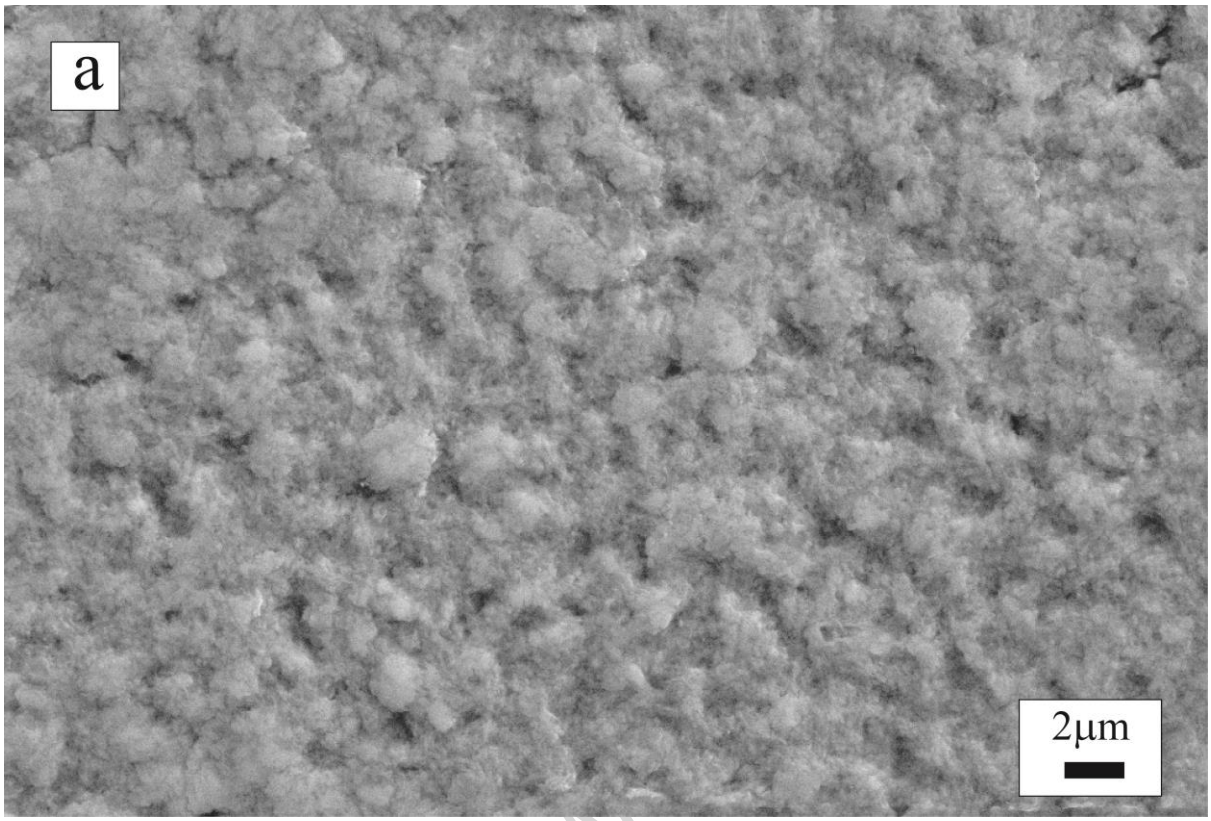

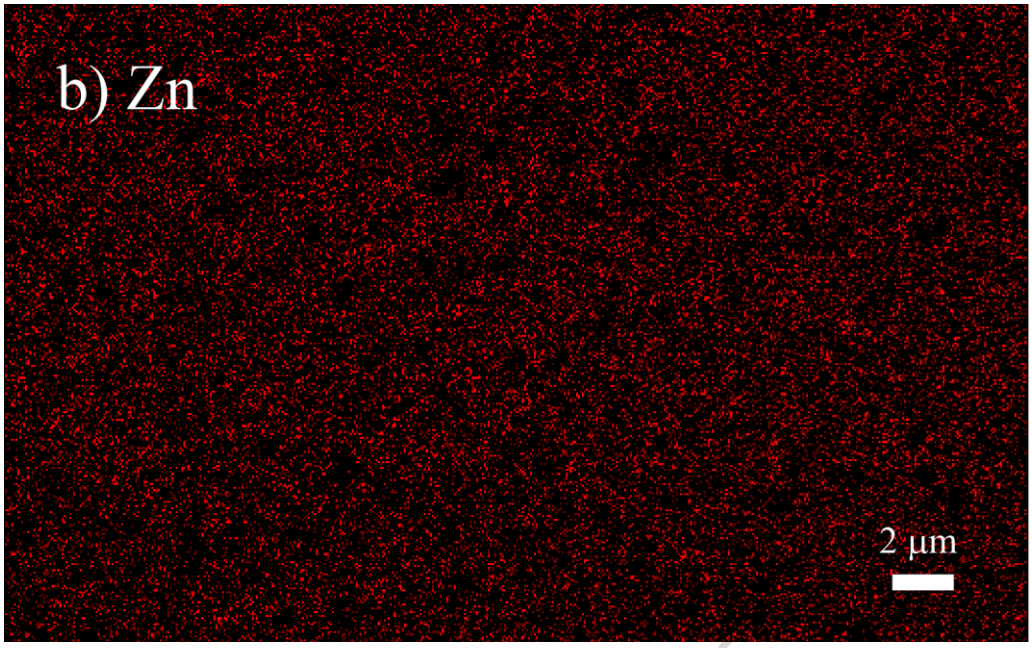

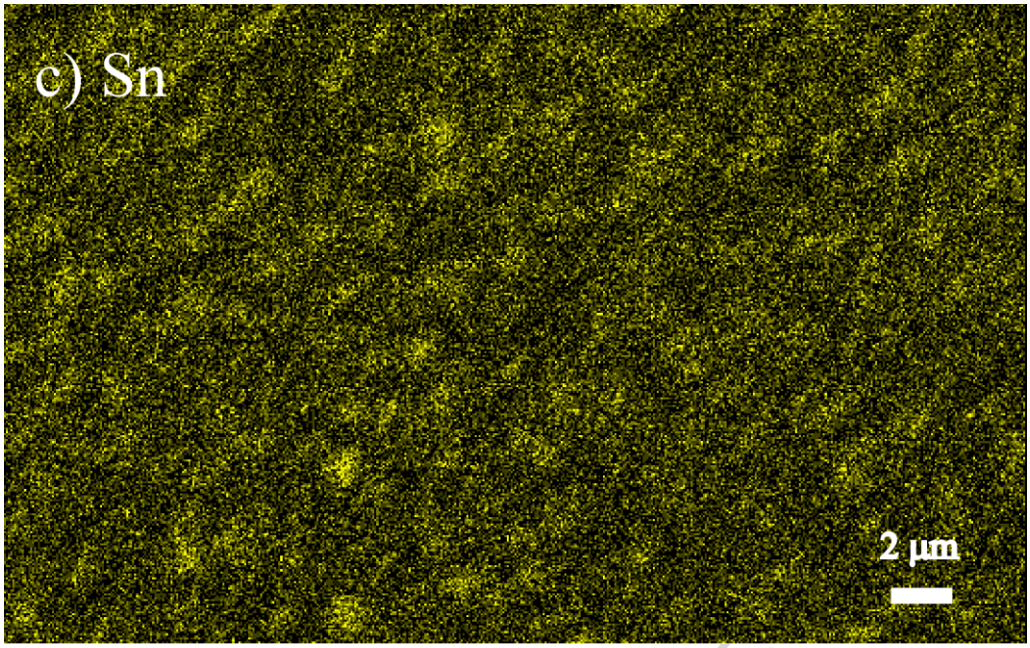

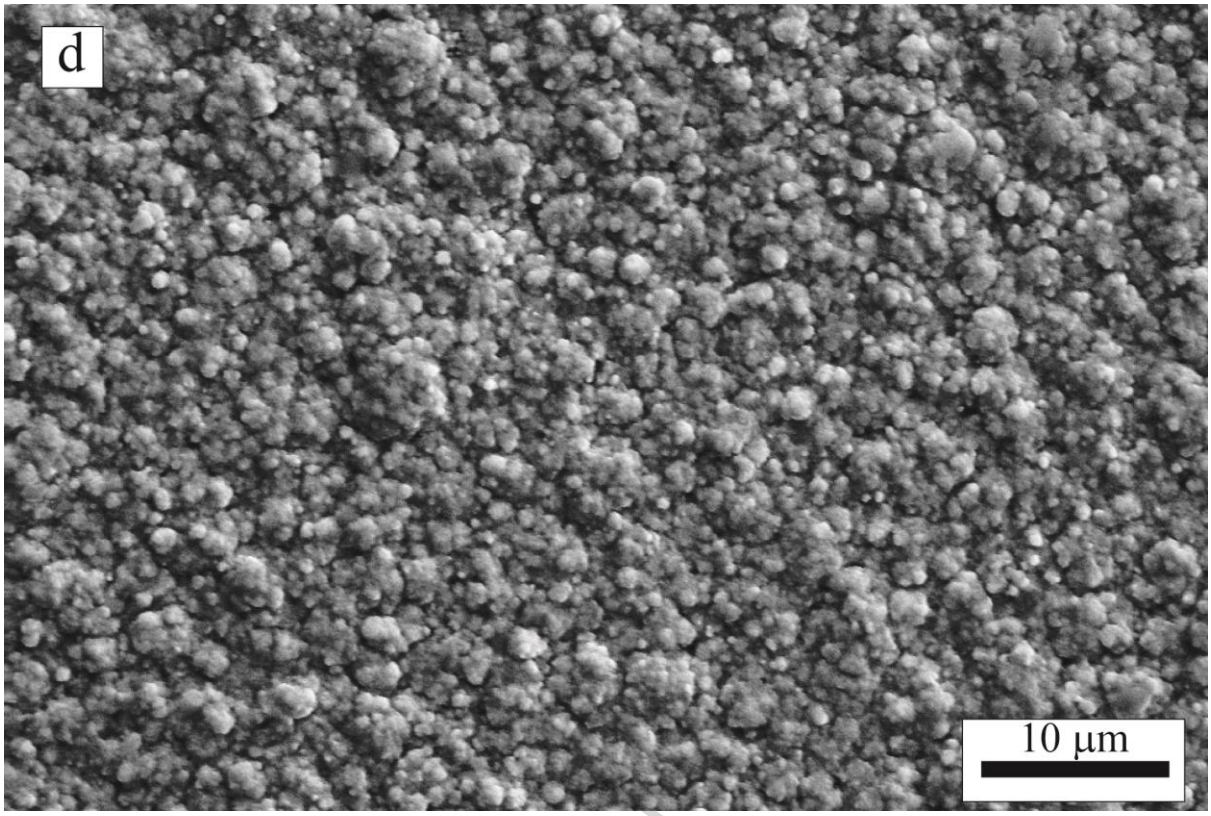

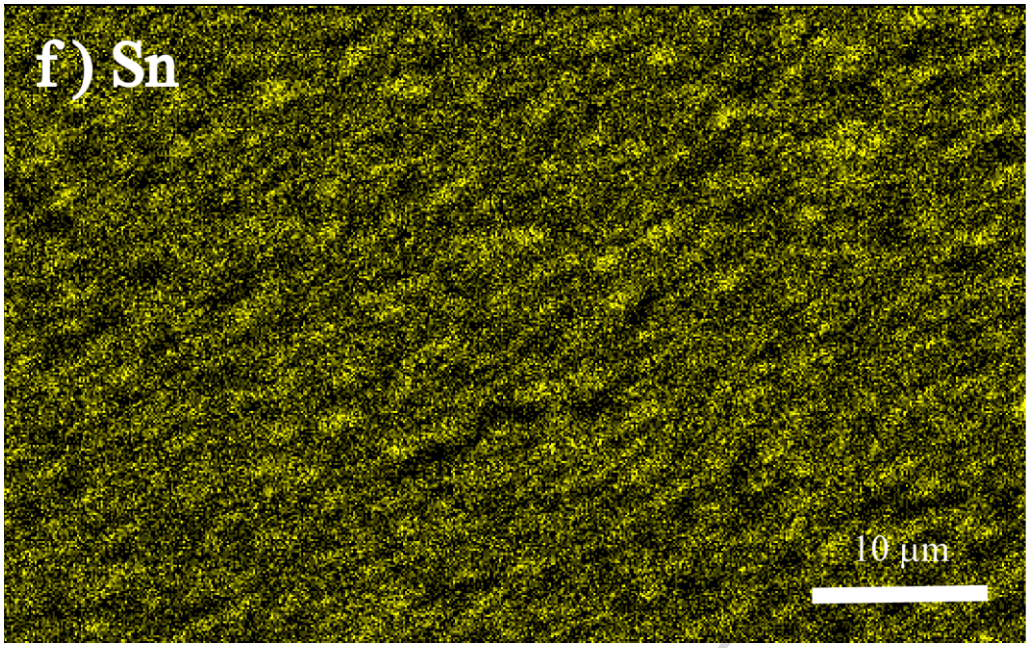

Fig. 5

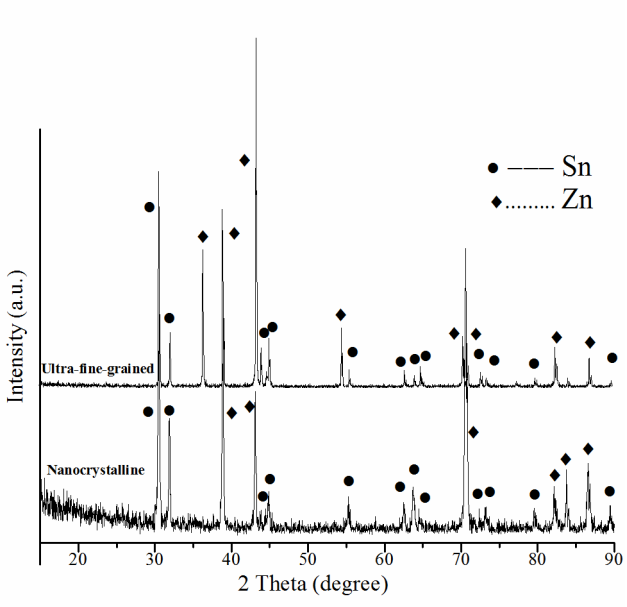

Fig. 6

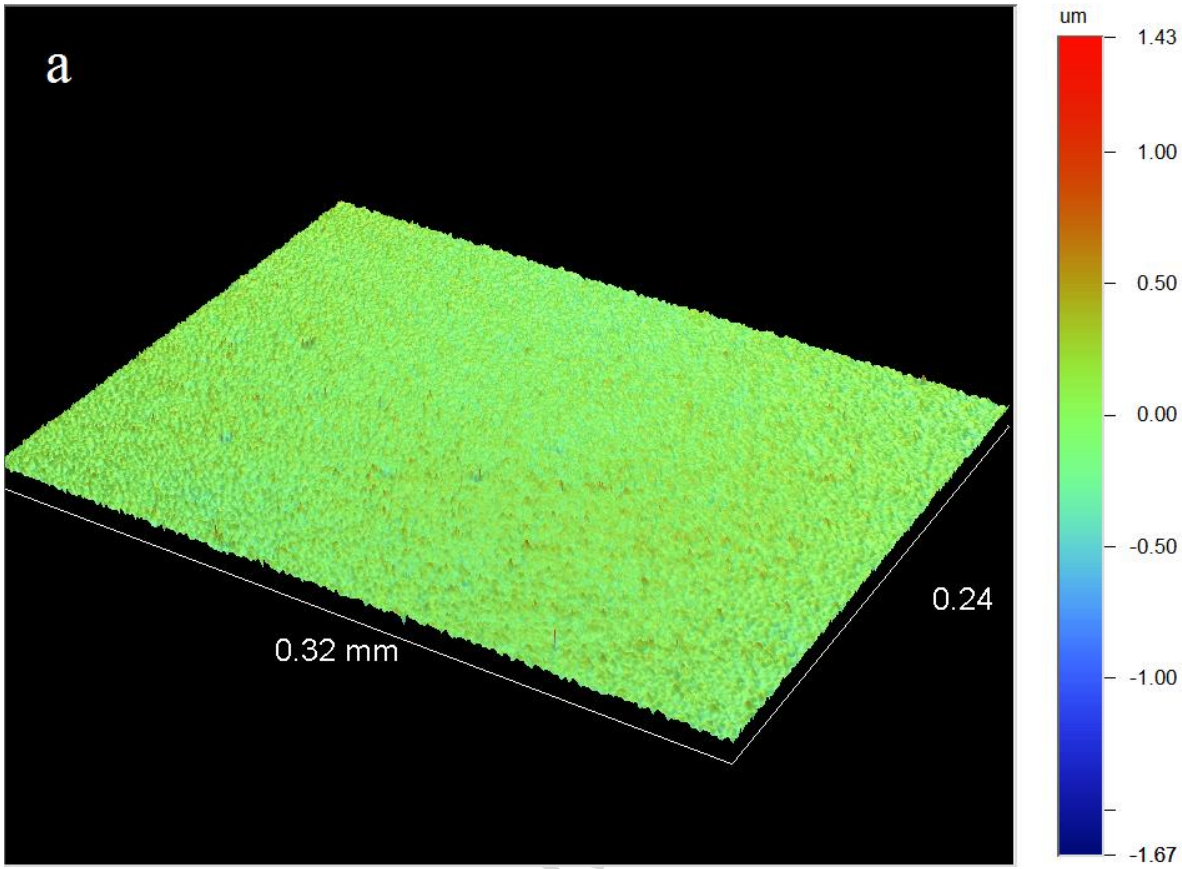

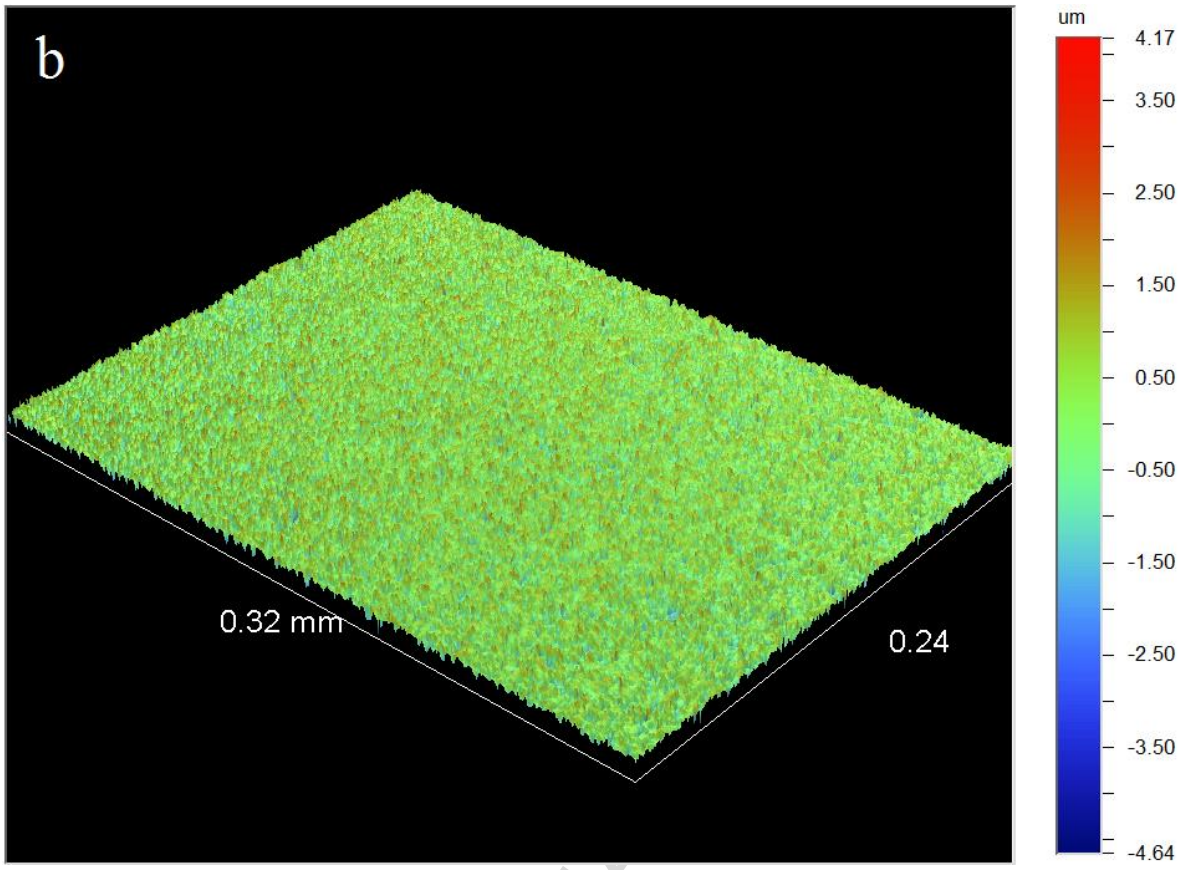

Fig. 7

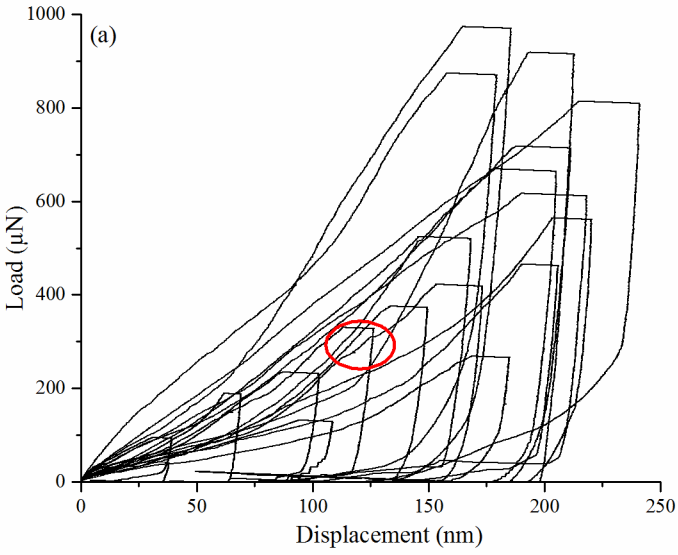

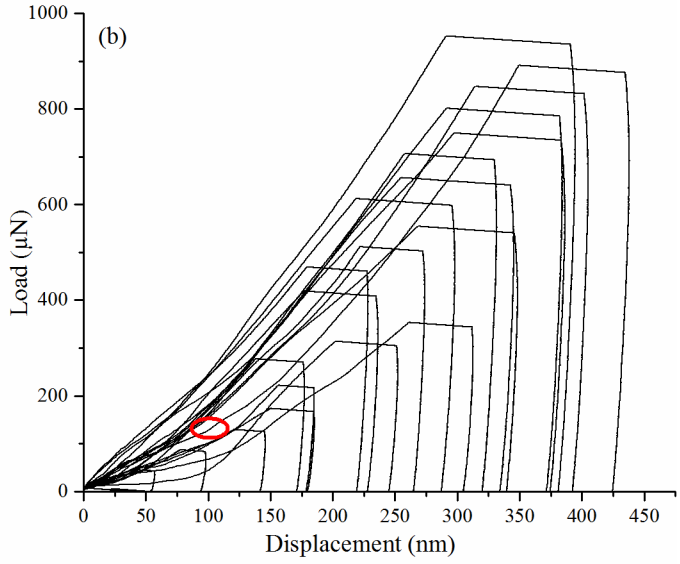

Fig. 8

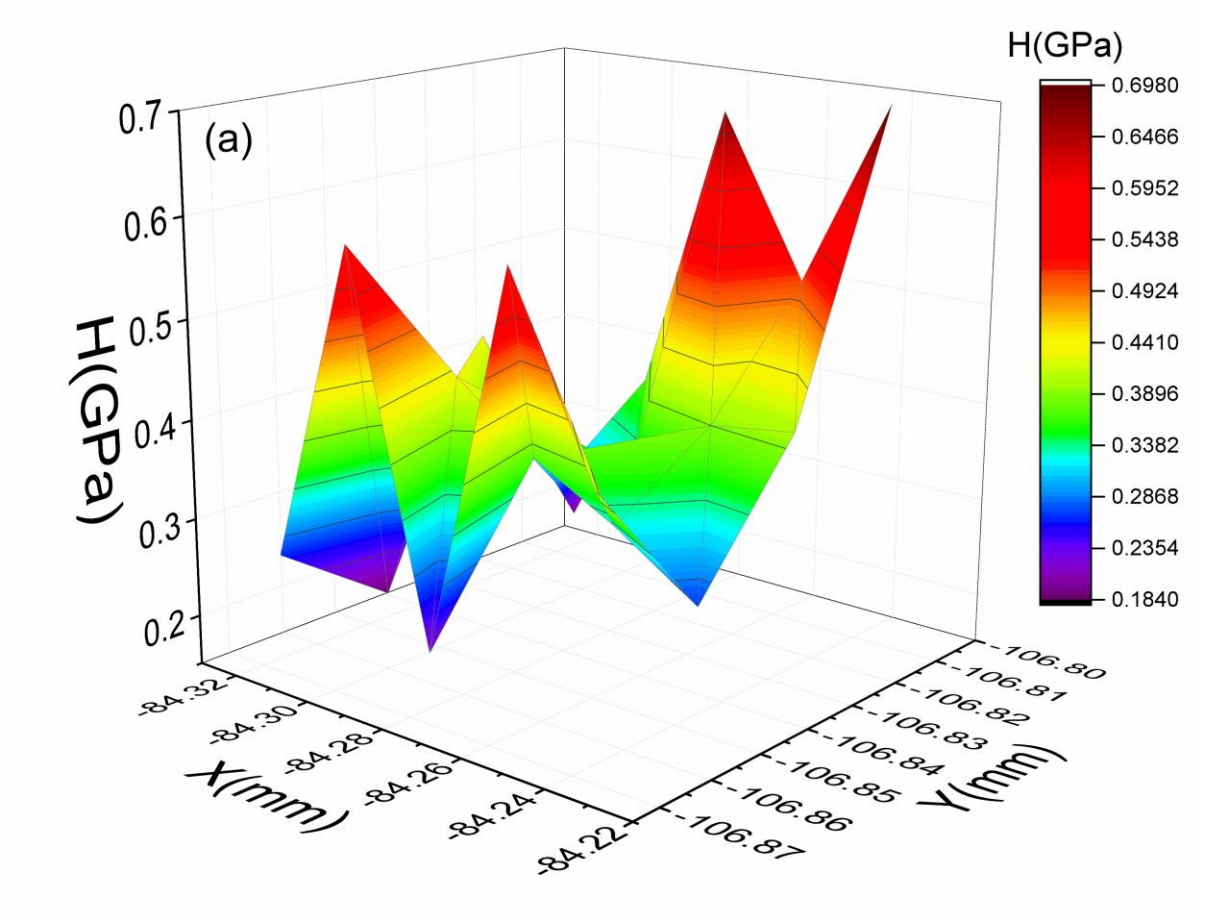

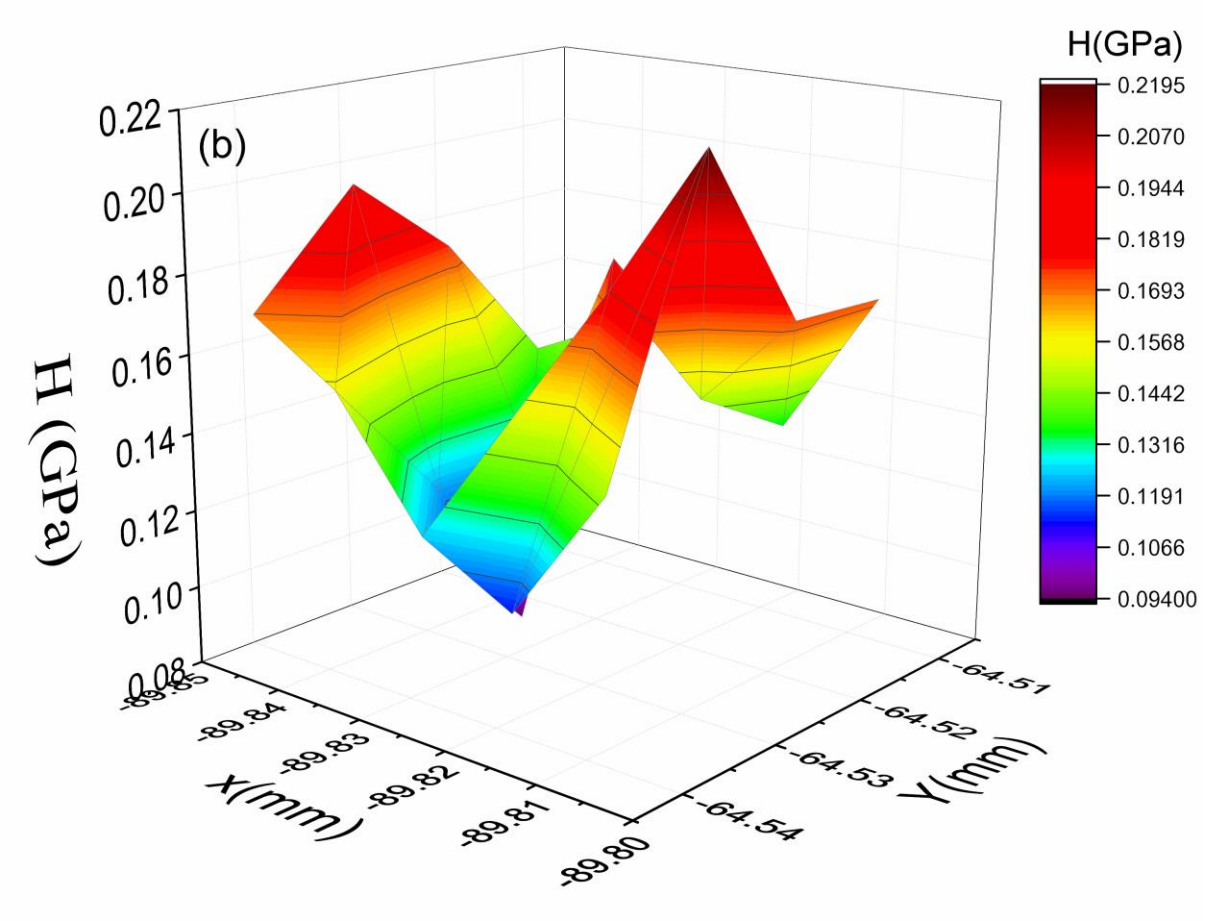

Fig. 9

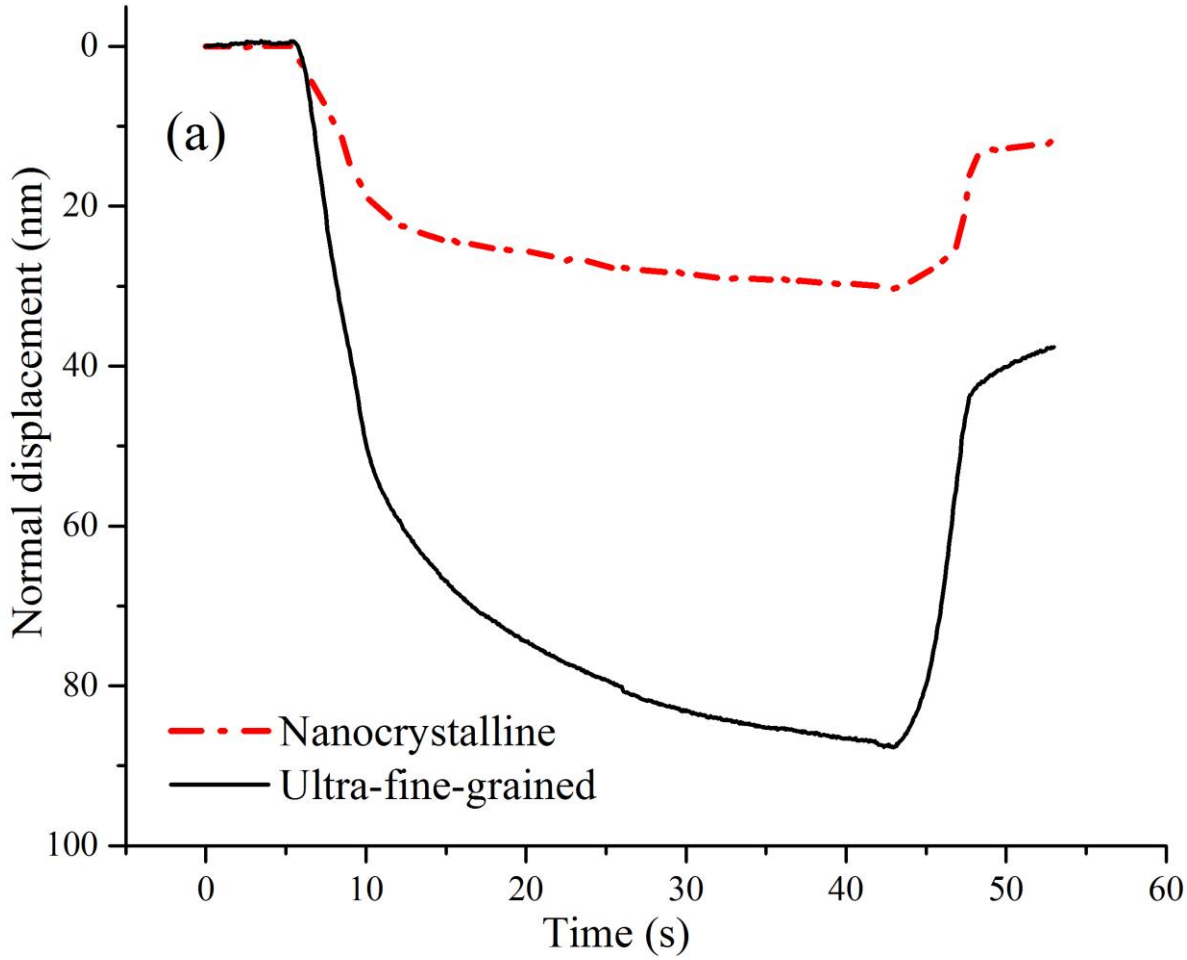

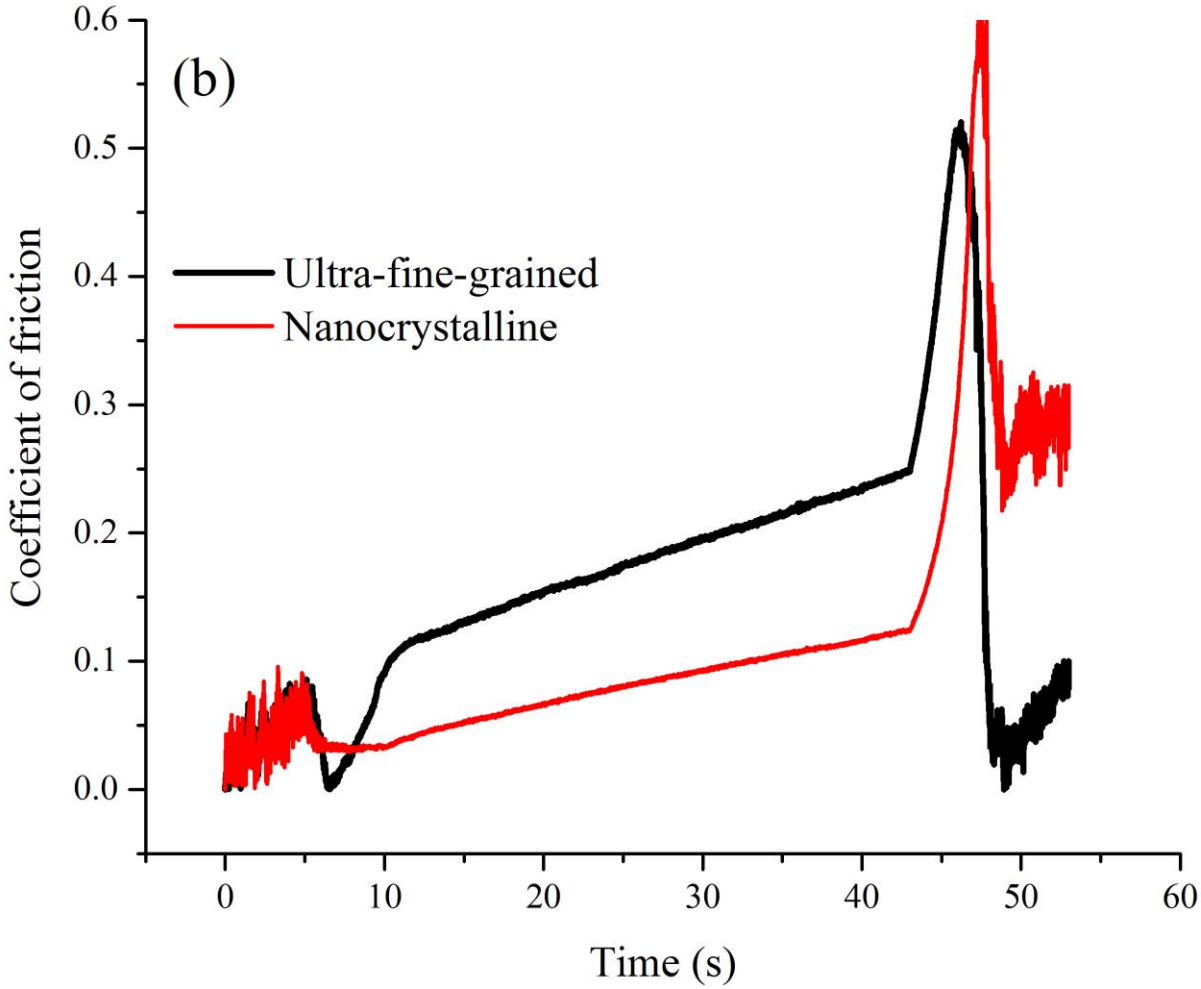

Fig. 10

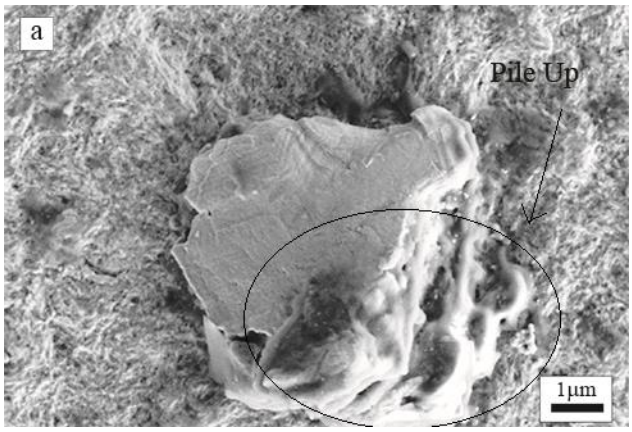

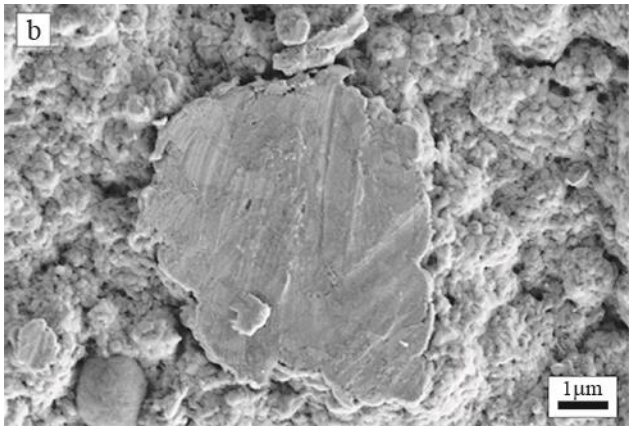

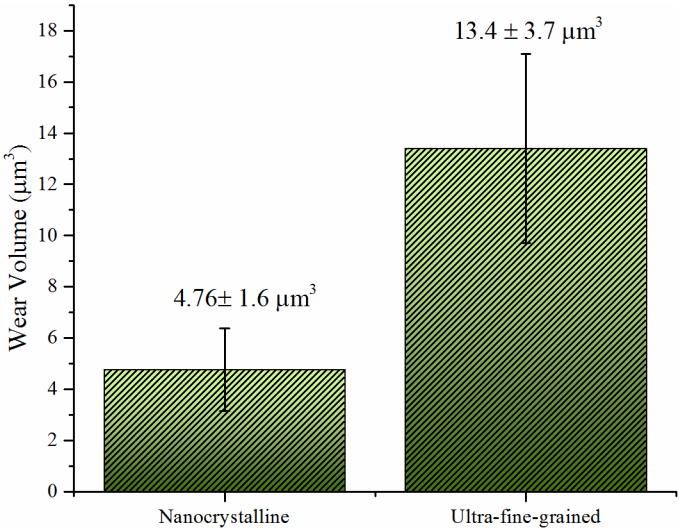

Highlights

- Nanocrystalline and ultrafine-grained Zn-Sn coatings were electrodeposited on steel substrates.
- Mechanical properties of nanocrystalline and ultrafine-grained coatings were compared.
- Grain refinement led to the improvement of Nano-hardness, nano-scratch and nano-wear properties of coatings.